water

Article

A Comprehensive Overview of the Hydrochemical Characteristics of Precipitation across the Middle East

Mojtaba Heydarizad [1], Luis Gimeno [2,*], Somayeh Amiri [3,4], Masoud Minaei [3,4] and Hamid Ghalibaf Mohammadabadi [5]

1 Faculty of Environment and Resource Studies, Mahidol University, Nakhon Pathom 73170, Thailand
2 Environmental Physics Laboratory (EphysLab), Facultad de Ciencias, Universidade de Vigo, 32004 Ourense, Spain
3 Department of Geography, Ferdowsi University of Mashhad, Mashhad 917794883, Iran
4 Geographic Information Science/System and Remote Sensing Laboratory (GISSRS: Lab), Ferdowsi University of Mashhad, Mashhad 917794883, Iran
5 Department of Geology, Ferdowsi University of Mashhad, Mashhad 917751436, Iran
* Correspondence: l.gimeno@uvigo.es

check for updates

Citation: Heydarizad, M.; Gimeno, L.; Amiri, S.; Minaei, M.; Mohammadabadi, H.G. A Comprehensive Overview of the Hydrochemical Characteristics of Precipitation across the Middle East. *Water* **2022**, *14*, 2657. https://doi.org/10.3390/w14172657

Academic Editor: Ataur Rahman

Received: 12 July 2022
Accepted: 25 August 2022
Published: 28 August 2022

Abstract: The Middle East is located in a semiarid and arid region and is faced with an intense water shortage crisis. Therefore, studying the hydrochemical characteristics of precipitation as a main part of the water cycle has great importance in this region. The hydrochemical analyses showed that the quality of precipitation was mainly affected by dust particles originating from terrestrial environments, while marine and anthropogenic sources had a minor role. The statistical studies showed that the dissolution of evaporative and carbonate minerals mainly controlled the hydrochemistry of precipitation. Precipitation had an acidic nature in some stations and a nonacidic nature in others. Ca^{2+} was the major acid-neutralizing cation in the Middle East precipitation. Various machine learning methods were also used to simulate the TDS values in precipitation. The accuracy of the developed models was validated, showing that the model developed by the Gboost method was more accurate than those developed by other machine learning techniques due to its higher R^2 values. To conclude, the hydrochemistry of precipitation showed significant variations across the Middle East. The dissolution of particles with terrestrial origins dominantly controlled the hydrochemistry of precipitation, while marine and anthropogenic sources had minor roles.

Keywords: hydrochemistry; precipitation; Middle East; ion sources; machine learning; statistics

1. Introduction

The Middle East is known as one of the main energy hubs in the world due to its large hydrocarbon reservoirs. However, this energy-rich zone has always faced significant water shortage crises due to successive intense droughts [1]. Furthermore, due to significant industrial and population growth in most parts of the Middle East in recent years, the importance of available water supplies and the need for new water resources have dramatically increased in this region [2]. Thus, accurate and reliable methods such as hydrochemical techniques besides statistical analyses should be applied to monitor water resources in this region. This can provide a comprehensive view of the quality and quantity of available water resources. In the hydrological cycle, the quality and quantity of precipitation (as an important element of the water cycle) should be studied very carefully due to its direct interactions with other elements that exist in the water cycle (e.g., surface water and groundwater resources). Although there are numerous studies on the quantity of precipitation and hydrological drought in the Middle East [3–9], few studies are available on the quality (hydrochemistry) of precipitation in this region [10–12].

During the last century, most parts of the world have undergone intense urbanization and industrialization. This has had a direct influence on the production and release of harmful gases (including SO_2 and NO_2). Therefore, the chemical properties of precipitation have been accurately studied in highly crowded and polluted metropolitan cities across the world, including Beijing in China [13], Tehran in Iran [14], Tokyo in Japan [15], Washington in the USA [16], Rio de Janeiro in Brazil [17], Sydney in Australia [18], and Delhi in India [19]. Studies on the hydrochemical characteristics of precipitation started earlier in the eastern part of Asia in Tokyo, Hanoi, Kolkata, Chennai, Sri Lanka, and East Java [20]. The study of the hydrochemical characteristics of precipitation in the western part of Asia and the Middle East was started by Salameh and Rimawi [11], Schemenauer and Cereceda [21], and Kattan [22] in the last three decades.

To study the hydrochemical characteristics of precipitation more deeply and accurately, statistical and machine learning techniques can be applied. Statistical techniques (such as principal component analysis (PCA), the Pearson correlation coefficient, and cluster analysis (CA)) have been applied in numerous studies to investigate the hydrochemical characteristics of precipitation [11,23–28]. In addition to statistical techniques, artificial intelligence (AI) techniques have also been applied in climatological studies, mainly in recent decades. Artificial neural network (ANN) techniques are a significant part of artificial intelligence. They have been designed based on the simulation of the human nervous system and have been applied in many fields of science. Although ANN techniques have existed for over half a century [29], their application in atmospheric sciences commenced in 1986 [30], and they have been mainly applied for forecasting the amount of precipitation [31–36]. The multilayer perceptron (MLP) model has one of the simplest and most efficient structures in ANN models and consists of three main parts, including an input layer, a hidden layer, and an output layer, which form a strong network [37]. In addition to simple ANN techniques, deep neural network (DNN) models have also been applied in numerous climatological studies [38,39]. The main difference between ANN and DNN models is the number of hidden layers. ANN models have only one hidden layer, while DNN models contain two or more hidden layers. In addition to neural network methods, data classification models such as decision trees and random forests have also been used to forecast the amount of precipitation [40–45]. A decision tree (DT) is a nonparametric supervised learning method. The aim of this method is to anticipate the value of the target parameter based on input parameters. In addition to the decision tree, a random forest, which is a combination of several decision trees and gradient boosting (an ensemble machine learning method), has also been used. The ensemble method is a machine learning technique that combines several basic machine learning methods to obtain an optimal predictive model. Although machine learning techniques have many advantages and capabilities in predicting the target parameter, there are still no studies on the simulation of precipitation quality using machine learning techniques.

This study aimed to investigate the hydrochemical characteristics of precipitation, including ion sources, enrichment factors, and neutralizing capacity, across the Middle East. In addition, statistical approaches and machine learning techniques were also employed to determine the main phenomena affecting the hydrochemistry of precipitation and to simulate the quality of precipitation (the values of total dissolved solids (TDS) in precipitation) using the concentrations of major ions in precipitation.

2. The Geography and Climatology of the Middle East

The Middle East is a region extending over a large area, including West Asia and North Africa. A large part of the Middle East is classified as a hot desert climate (BWh) according to the Köppen climate zone. However, other climate zones such as BSk (arid, steppe, and cold), Csa (temperate, dry summer, and hot summer), BWk (arid, desert, and cold), and BSh (arid, steppe, and hot) are also observed in some areas of this region [46]. Significant variations in temperature and precipitation observed across the Middle East also confirm the existence of various climate zones [47–49]. Precipitation moisture in the Middle East is transferred by five main air masses, including continental polar (cP), maritime polar (mP), maritime tropical (mT), Mediterranean (MedT), and continental tropical (cT) air masses (Figure 1).

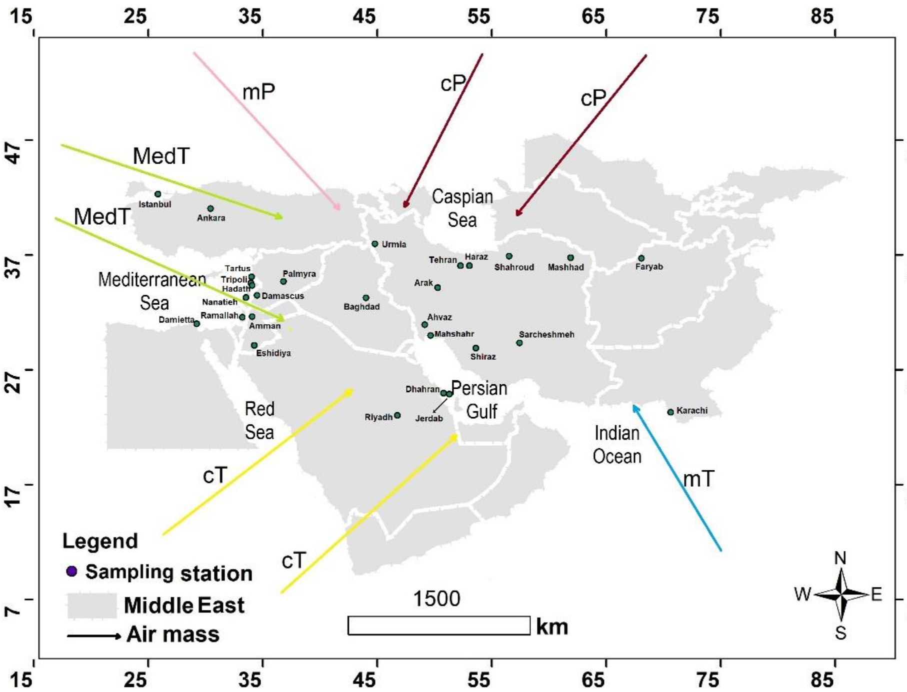

Figure 1. The studied stations and main air masses affecting the Middle East.

Air mass flux and moisture sources have also been studied using vertically integrated moisture flux (VIMF) (Figure 2). The northward and eastward data of the vertically integrated moisture flux from ERA-Interim reanalysis [50] with a resolution of 1° × 1° were utilized in this study. ERA-Interim reanalysis belongs to the European Center for Medium-Range Weather Forecast (ECMWF). During the dry period (May to October) in the Middle East, a notable VIMF can be observed over the Indian Ocean and the Arabian Sea. During this period, the VIMF divergence can also be seen at degrees higher than 40 °N. In contrast, during the wet period (from November to April), the VIMF convergence prevails over the Middle East and causes precipitation. During this period, moisture mainly originates from the Mediterranean Sea, the Black Sea, the Persian Gulf, and the Arabian Sea. This is in close agreement with previous studies [51,52].

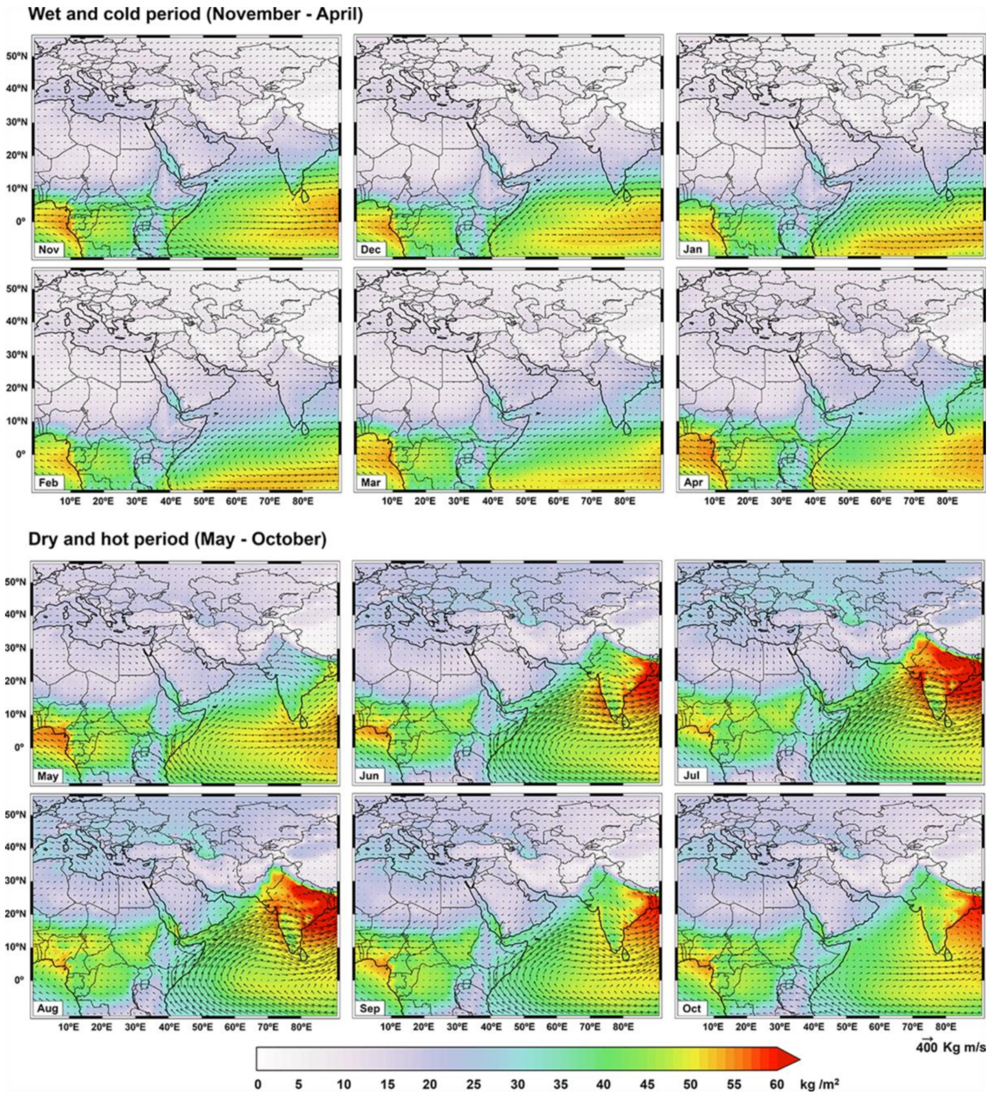

Figure 2. The northward and eastward data of the vertically integrated moisture flux (VIMF) with a 1° × 1° resolution from 1981 to 2021 are derived from ERA-Interim reanalysis [53].

3. Materials and Methods

In this study, the data of hydrochemical analyses (including field parameters (pH, TDS, and electrical conductivity (EC)) and the major and minor ions) were studied in 28 stations across the Middle East. These stations and their hydrochemical analyses in Shiraz [54], Ahvaz [26], Mahshahr [55], Sarcheshmeh [56], Tehran [24], Mashhad [57], Arak [28], Shahroud [58], Haraz [12], and Urmia [59] in Iran; Riyadh [60] and Dhahran [21] in the Kingdom of Saudi Arabia (KSA); Damietta in Egypt [61]; Karachi in Pakistan [62]; Ramallah [63] in Palestine; Tripoli, Hadath, and Nabatieh in Lebanon [64]; Jerdab [65] in Bahrain; Tartus, Palmyra, and Damascus in Syria [22]; Amman [11] and Eshidiya [27] in Jordan; Ankara [66] and Istanbul [67] in Turkey; Baghdad in Iraq [68]; and Faryab [69] in Afghanistan were chosen from the scientific papers in the literature.

In most of the stations, samples from precipitation events were collected in polyethylene bottles. The field parameters, including pH, TDS, and EC, were measured up to 24 h after precipitation. Hydrochemical analyses of the precipitation samples were conducted in various laboratories across the world, including the Acme Analytical Lab in Canada; the physical chemistry laboratory of the Faculty of Sciences at the Ferdowsi University of Mashhad, Iran; the laboratory of the Shiraz Regional Water Authority, Iran; British Geological Survey (BGS) laboratories, England; the environmental engineering laboratory at Fatih University, Turkey; and some other laboratories across the Middle East. The concentrations of most major anions, including NO_3^-, SO_4^{2-}, and Cl^-, were measured using an ion chromatography instrument, while the concentrations of most cations, including K^+, Ca^{2+}, and Mg^{2+}, were measured by a flame atomic absorption spectrophotometer. The concentration of HCO_3^- was measured using titration with 0.01 M hydrochloric acid. Using the Nessler method, the concentration of NH_4^+ was also measured only in a few stations, such as Eshidiya [70].

The differences in the methods of sampling and hydrochemical analysis have a direct effect on the uncertainty of the analyses and the accuracy of the study. Thus, a charge balance error (CBE) index was calculated and used to evaluate the accuracy of the hydrochemical analysis of precipitation as follows:

$$\text{CBE } (\%) = \frac{\sum(cations - anions)}{\sum(cations - anions)} \times 100 \quad (1)$$

A hydrochemical analysis with a CBE of <5% confirms that the dataset is reliable. The CBE values show large variations from 0.8% in Faryab station to 6.5% in Ankara station, with an average of 3.99% in all stations across the Middle East. Figure 3 also demonstrates the variations in CBE in the precipitation analyses in the studied stations. Since the concentrations of the major anions and cations were not completely presented in some of the studied stations, the CBE (%) was not calculated for them.

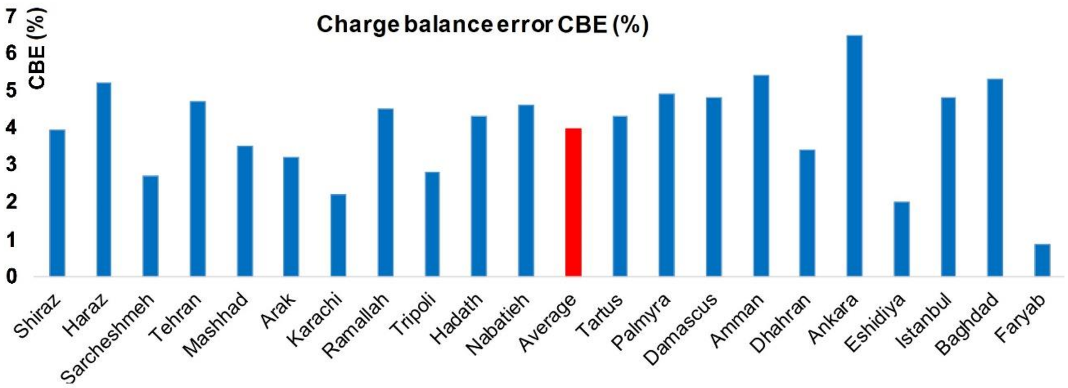

Figure 3. The variations in CBE (%) calculated for the precipitation analyses in the studied stations across the Middle East.

First, in order to estimate the marine and nonmarine origins of precipitation, sea salt fraction (SSF) and nonsea salt fraction (NSSF) indices were calculated in precipitation using Equations (2) and (3), respectively [71].

$$SSF_x = [Na^+{}_{rain}] \times [X/Na^+]_{seawater} \quad (2)$$

$$NSSF_x = [X_{rain}] - [(Na^+{}_{rain}) \times (X/Na^+)_{seawater}] \quad (3)$$

Using Equation (4), an enrichment factor (EF) was also calculated to study the origin of the ionic species Ca^{2+}, Na^+, K^+, HCO_3^-, SO_4^{2-}, and Cl^- with respect to Na^+ [72].

$$EF_{seawater} = [X/Na^+]_{rainwater} \;/\; [X/Na^+]_{seawater} \quad (4)$$

In the above equations, X represents the ion of interest. Since Na^+ is assumed to originate totally from the sea [73,74], it is used as a reference for marine sources.

The acidity of precipitation was also considered by calculating the fractional acidity (FA) using Equation (5) [75]:

$$FA = [H^+] \;/\; ([NO_3^-] + [NSS_{SO4}{}^{2-}]) \quad (5)$$

$NSS_{SO4}{}^{2-}$ and $NO_3{}^{-}$ (eq/lL) are two dominant acidic components in the above equation, while H^+ is calculated by Equation (6) using pH values.

$$[H^+] = 10^{-pH} \text{ (eq/l)} \tag{6}$$

In addition to the neutralization process in the studied stations, a neutralization factor (NF), considered an indicator of the neutralization potential in the precipitation samples, was also calculated for some of the major alkaline species (Ca^{2+}, Mg^{2+}, $NH_4{}^+$, and K^+) in precipitation using Equations (7)–(10) [73].

$$NF_{Ca}{}^{2+} = [NSS_{Ca}{}^{2+}] / ([NO_3{}^{-}] + [NSS_{SO4}{}^{2-}]) \tag{7}$$

$$NF_{Mg}{}^{2+} = [NSS_{Mg}{}^{2+}] / ([NO_3{}^{-}] + [NSS_{SO4}{}^{2-}]) \tag{8}$$

$$NF_{K}{}^{+} = [NSS_{K}{}^{+}] / ([NO_3{}^{-}] + [NSS_{SO4}{}^{2-}]) \tag{9}$$

In the above equations, NSSx is the contribution of a nonsea salt fraction to any desired ion (X) in the precipitation samples.

Finally, statistical analyses and machine learning algorithms were used to comprehensively study the possible sources of ions in the Middle East precipitation. $NH_4{}^+$ and $NO_3{}^-$ were omitted from the statistical analyses since there were no data about these ions (NA) in some of the studied stations. However, missing $HCO_3{}^-$ concentrations or pH data in some stations were calculated based on the following empirical equation [73,76,77].

$$[HCO_3{}^{-}] = 10^{-11.24+pH} \text{ (eq/l)} \tag{10}$$

PCA was applied to the precipitation datasets. PCA is a statistical technique for reducing the dimensionality of large datasets. This increases interpretability and minimizes information loss in datasets [78]. To achieve this goal, PCA uses factor extension with an eigenvalue of >1 after applying varimax rotation. The PCA used in this study was performed in the R programming language by R software version 4.1.3. [79].

In addition, ANN and DNN techniques, as well as other machine learning algorithms such as random forest, decision tree, and gradient boosting (Gboost), were also used for two goals. The first goal was to determine which ions mainly control the hydrochemistry of precipitation (the TDS values) by presenting the importance percentage of each major ion influencing the TDS values. The second goal was to simulate the TDS values in precipitation based on the concentrations of the major ions. The accuracy of the developed models was validated by the coefficient of determination (R^2).

4. Results and Discussion

4.1. The Hydrochemical Characteristics of Precipitation across the Middle East

The hydrochemical parameters across the Middle East show large variations. Among the field parameters, pH varies from 4.7 at Ankara station to 7.8 at Mashhad station. In previous studies [80–82], water from a clean and unpolluted atmosphere had a pH of about 5.6 [23]. However, the precipitation events with a pH lower than 5.6 demonstrate anthropogenic acidity mainly caused by NO_2 and SO_2 gases originating from coal burning, fuel combustion in car engines, and industrial activities [23,81]. Very low pH values at Ankara station are due to the highly polluted atmosphere in this city, mainly owing to automobile fuel combustion, intense industrial activities, and coal burning [83]. Fuel combustion in cars and industrial factories has a direct effect on the production and release of SO_2 and NO_2 gases, which contribute to precipitation acidity by producing H_2SO_4 and HNO_3, respectively [47]. In other large and crowded metropolitan cities in the Middle East such as Istanbul, Tehran, and Karachi, the pH values are low to moderate (5.1, 6.3, and 6.8, respectively). As another field parameter, EC also shows large variations across the Middle East, ranging from 56 µmho/cm at Shahrood station to 310 µmho/cm at Jerdab (Jurdab) station. The high EC values at Jerdab station may be due to the existence of significant amounts of dust particles in the desert air. There are no anthropogenic sources, such as heavy traffics or industrial zones, in this region. Therefore, the dust particles originating from large deserts in this region are the main reason for high EC values in precipitation. The role of dust particles and aerosols in the quality of the atmosphere in this region has been previously studied in several papers [84–86]. The precipitation events at other stations located in the desert such as Riyadh and Damietta also show high EC values (226 μmho/cm and 289 μmho/cm, respectively). TDS, which is another field parameter and is highly correlated to EC, also shows large variations across the Middle East. The TDS values range from 56 mg/l at Tehran station to 156 mg/l at Jerdab station. The high EC and TDS values at Jerdab station, located in the desert, are due to the significant amount of dust particles in the atmosphere at this station. Other stations that are located in the desert or near it such as Palmyra, Baghdad, and Damietta also show high TDS values due to the significant amounts of dust particles in their atmospheres.

In addition to the field parameters, the average concentrations of the major and some minor ions in the Middle East precipitation were also studied (Figure 4). Among the cations, Ca^{2+} shows the highest average concentration in precipitation, varying from 1.6 mg/l at Eshidiya station to 52.9 mg/l at Ankara station. The Ca^{2+} ion has a mainly terrestrial origin. This ion mainly originates from evaporative (gypsum ($CaSO_4 \cdot 2H_2O$) and anhydrite ($CaSO_4$)) and/or carbonate minerals (calcite ($CaCO_3$), dolomite (Ca Mg $(CO_3)_2$), and aragonite ($CaCO_3$)). Na^+ is the second dominant ion in the Middle East precipitation. The concentration of this ion in precipitation ranges from 1.6 mg/l at Sarcheshmeh and Damascus stations to 23.9 and 23.4 mg/l at Mashhad and Mahshahr stations, respectively. The highest concentration of Na^+ at Mashhad station is not completely clear yet. However, this ion may originate from Na-containing minerals, such as halite (NaCl) and albite ($NaAlSi_3O_8$), which exist in the Ngr Formation in nearby regions [87]. The high concentration of Na^+ at the coastal station of Mahshahr is due to its marine sources from the Persian Gulf. K^+ and Mg^{2+} show much lower concentrations in precipitation than Ca^{2+} and Na^+. The concentration of Mg^{2+} in precipitation varies from 0.4 mg/l at Sarcheshmeh station to 9.7 mg/l at Arak station. The high values of Mg^{2+} in precipitation are mainly due to its marine origin. However, it can also originate from dust particles with Mg-containing minerals, such as epsomite ($MgSO_4 \cdot 7H_2O$) and magnesite ($MgCO_3$). Since Arak station is located deep in the continent, Mg^{2+} dominantly originates from dust particles from terrestrial sources. The existence of marl and marl-intercalated limestone near Arak station [88] also confirms this idea. The K^+ ion in the Middle East precipitation also varies from 0.4 mg/l at Dhahran station to 9.4 mg/l at Sarcheshmeh station. The K^+ ion may have marine and/or terrestrial sources. Because Sarcheshmeh station is located deep in the continent, the K^+ ion in the precipitation samples in this station originates from dust particles from the Sarcheshmeh copper mine complex, which is located nearby. $NH_4{}^+$ is another important cation in the precipitation samples. The concentration of this ion was analyzed for some of the stations. It varies from 0.3 mg/l at Ahvaz station to 21.7 mg/l at Ankara station. In contrast to other cations with mainly terrestrial or marine sources, this ion mainly originates from anthropogenic sources. The high concentration of $NH_4{}^+$ in the precipitation at Ankara station is due to intense agricultural activities in the surrounding areas not only in spring but also in autumn and winter. These intense agricultural activities have neutralized precipitation [66].

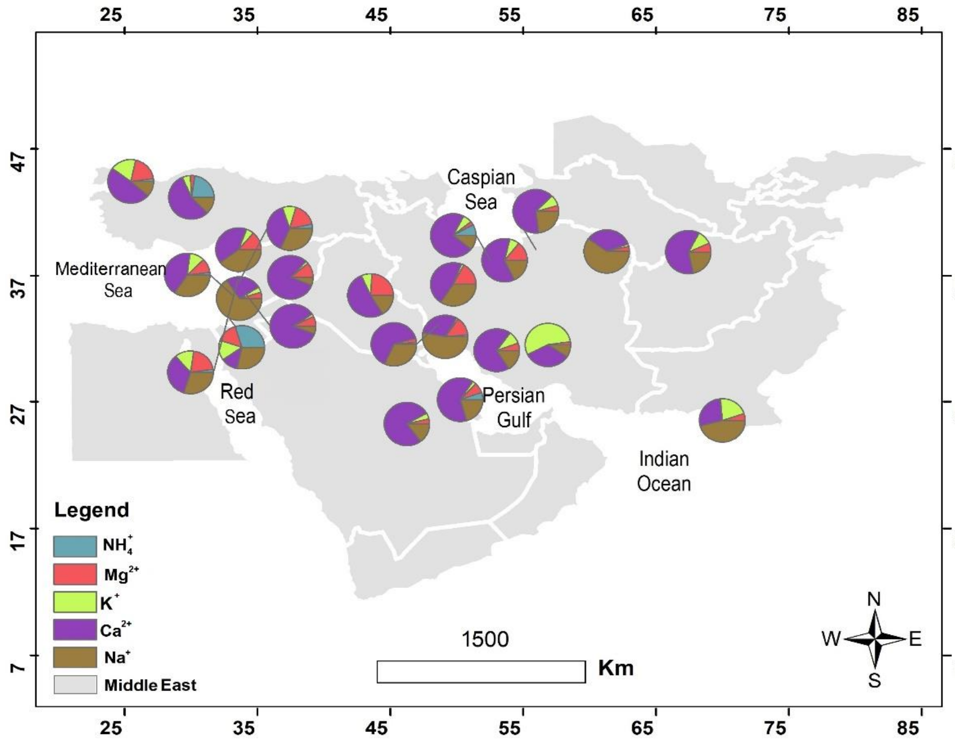

Figure 4. The variations in major cations in the precipitation at the studied stations across the Middle East.

Among the anions, SO_4^{2-} and HCO_3^- have higher concentrations and a more important role in the chemistry of precipitation (Figure 5). The concentration of SO_4^{2-} in precipitation varies from 1.1 mg/l at Hadath station to 143.5 mg/l at Damietta station. The extremely high concentration of SO_4^{2-} is due to significant air pollution in the region caused by several factors, such as textile factories, painting and furniture activities, and heavy traffic [61]. The concentration of HCO_3^-, which is another important anion in the Middle East precipitation, varies from 0.4 mg/l at Shiraz station to 146.4 mg/l at Ankara station. The high concentrations of HCO_3^- are accompanied by high concentrations of Ca^{2+} in the precipitation samples at Ankara station. This is due to two possible reasons: first, the dissolution of very high amounts of CO_2 in precipitation originating from the burning of fossil fuels in automobiles; second, the dissolution of limestone dust particles rich in $CaCO_3$ in the precipitation samples of this station [89]. The concentration of the Cl^- ion in the Middle East precipitation also varies from 2.2 mg/l at Haraz station to 51.8 mg/l at Ankara station. The Cl^- ion mainly originates from marine sources, but can also originate from anthropogenic sources, including exhaust fumes, fertilizers, and the burning of coal [13,90]. The high concentrations of Cl^- at Ankara, as a crowded and polluted city, may have both marine and anthropogenic origins. Finally, the NO_3^- ion shows large variations, from 0.1 mg/l at Jerdab station to 136.4 mg/l at Ankara station. NO_3^- is a conservative ion that mainly originates from anthropogenic sources. Among the studied stations in the Middle East, Ankara and Damietta show the highest concentrations of NO_3^- (136.4 and 103.6 mg/l, respectively). The significantly high concentrations of NO_3^- in the air of these cities are due to industrial activities as well as heavy traffic, which add large amounts of air pollutants to the atmosphere of Ankara [66] and Damietta [61].

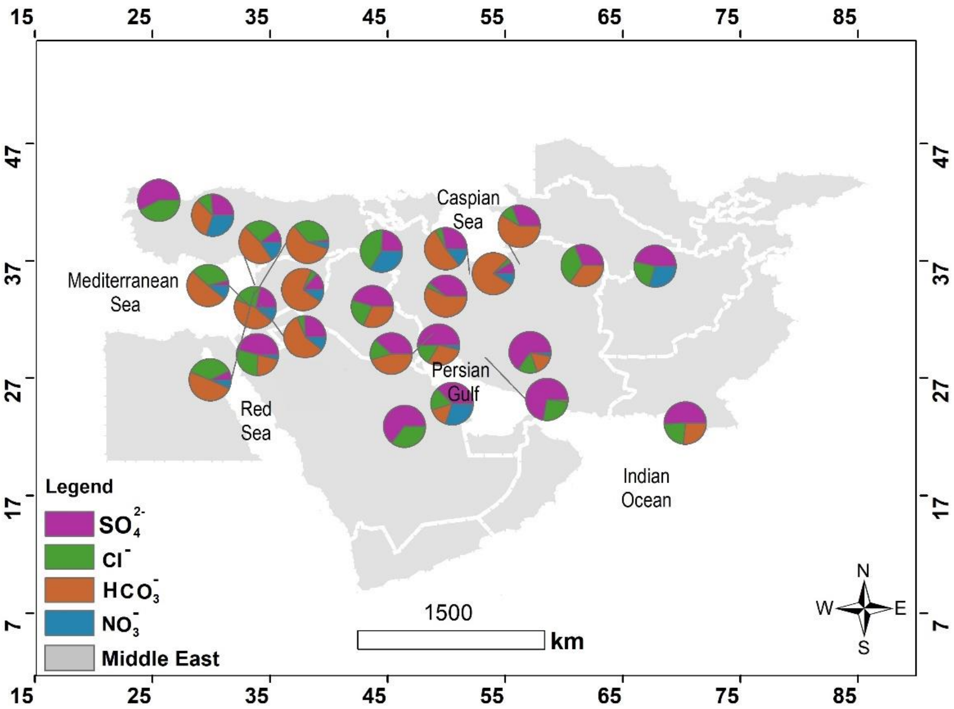

Figure 5. The variations in the major anions in the precipitation at the studied stations across the Middle East.

Based on their locations, the precipitation in the studied stations also demonstrates several water types. The stations located on the Mediterranean Sea coast (e.g., Tripoli, Istanbul, and Tartus) or its vicinity (e.g., Nabatieh and Hadath) show a $CaCl_2$ water type. The precipitation events in the stations located on the Persian Gulf coast (e.g., Mahshahr and Dhahran) demonstrate $NaSO_4$ and $CaSO_4$ water types, while those at Ahvaz station (near the Persian Gulf) show a $CaSO_4$ water type. Finally, the precipitation at Karachi station, located on the Oman Sea coast, shows a $NaSO_4$ water type. These water types are normal in coastal areas due to the mainly marine origins of the SO_4^{2-}, Cl^-, and Na^+ ions. Several water types are observed in the continental stations across the Middle East. At Tehran, Riyadh, Shiraz, Ankara, and Sarcheshmeh stations, the dominant precipitation water type is $CaSO_4$. However, at Damascus, Palmyra, Shahroud, Ahvaz, and Arak stations, the dominant precipitation water type is $CaHCO_3$. The $CaSO_4$ and $CaHCO_3$ water types in the precipitation at most continental stations across the Middle East are due to the dominant role of ions with terrestrial origins. The carbonate aerosol particles originating from carbonate formations increase the concentrations of Ca^{2+}, Mg^{2+}, and HCO_3^- ions in precipitation. However, the particles originating from evaporative minerals, which have large outcrops in the Middle East, significantly increase the concentrations of Ca^{2+} and SO_4^{2-} [26,54,91]. At other continental stations, including Ramallah, Amman, and Eshidiya, $NaNO_3$, $NaHCO_3$, and NH_4SO_4 are the dominant water types, respectively. Both Ramallah and Amman are located near the Dead Sea in the Jordan Rift Valley. The Na^+ ion in the precipitation at these stations originates from salt particles from the highly saline Dead Sea. The NH_4SO_4 water type in the precipitation at Eshidiya station is due to anthropogenic pollution in the atmosphere of this station, mainly caused by industrial (e.g., by Indo-Jordan Chemicals) and mine activities in this area. Eshidiya is a polluted area, and the approximately high concentrations of NO_3^-, NH_4^+, and SO_4^{2-} ions (63.7, 43.0, and 121.5 μeq/l, respectively) in the precipitation at this station show it [27].

4.2. The Origins of the Major Ions in Precipitation in the Middle East

The chemistry of precipitation is controlled by different factors, including terrestrial, anthropogenic, and marine sources. Studying the ratio of major ions to Na^+ and Ca^{2+} shows marine and crust sources, respectively, whereas the SO_4^{2-}/NO_3^- ratio can provide valuable information about the anthropogenic sources of ions in precipitation (Supplementary Table S1). The SO_4^{2-}/Na^+, K^+/Na^+, Ca^{2+}/Na^+, and Mg^{2+}/Na^+ ratios in precipitation at the studied stations across the Middle East (Figure 6) are higher than seawater ratios [92]. The higher average ratios in precipitation compared with seawater ratios demonstrate that in addition to marine sources, anthropogenic and terrestrial sources also affect the chemical characteristics of precipitation.

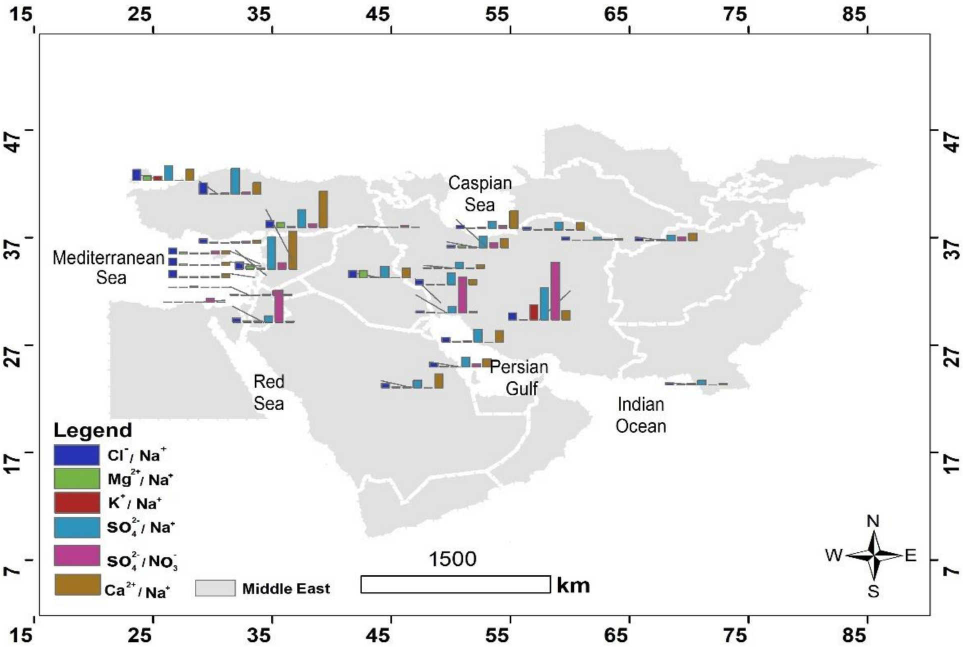

Figure 6. The distribution of major ion ratios in precipitation to Na^+ and $SO4^{2-}/NO^{3-}$ in the studied stations.

The ratios of major ions to Ca^{2+} (including SO_4^{2-}/Ca^{2+}, K^+/Ca^{2+}, Na^+/Ca^{2+}, and Mg^{2+}/Ca^{2+}) present important information about the role of ions from the crust in precipitation (Figure 7). The X/Ca^{2+} ratio has lower values at continental stations than at marine stations. This is due to the fact that the role of the crust in the chemistry of precipitation increases toward the continental stations; the concentration of Ca^{2+} as an indicator of crust/terrestrial origin increases, while the X/Ca^{2+} ratio decreases toward the continent. There are some exceptions among the continental stations, such as Eshidiya station. Although it is located on the continent, it shows high X/Ca^{2+} ratios. This is perhaps due to severe anthropogenic pollution at this station, as was mentioned above.

Furthermore, the SO_4^{2-}/NO_3^- ratio is a good indicator for studying and monitoring anthropogenic sources in precipitation [93]. In the Middle East precipitation, this ratio varies from 0.37 to 21.77, with an average of 3.77. Both SO_4^{2-} and NO_3^- contribute to precipitation acidity by producing H_2SO_4 and HNO_3, respectively [94]. At most stations across the Middle East, the SO_4^{2-}/NO_3^- ratio is very low. For instance, at Tehran and Ankara stations, which are affected by severe air pollution, the SO_4^{2-}/NO_3^- ratio is 1.94 and 0.88, respectively. Atmospheric pollution due to fuel combustion in vehicles and the lower usage of other air pollutants, such as coal, result in low SO_4^{2-}/NO_3^- ratios [26]. However, higher values of SO_4^{2-} compared with NO_3^- in precipitation acidity have also been reported in areas where coal is used to provide energy [10,95].

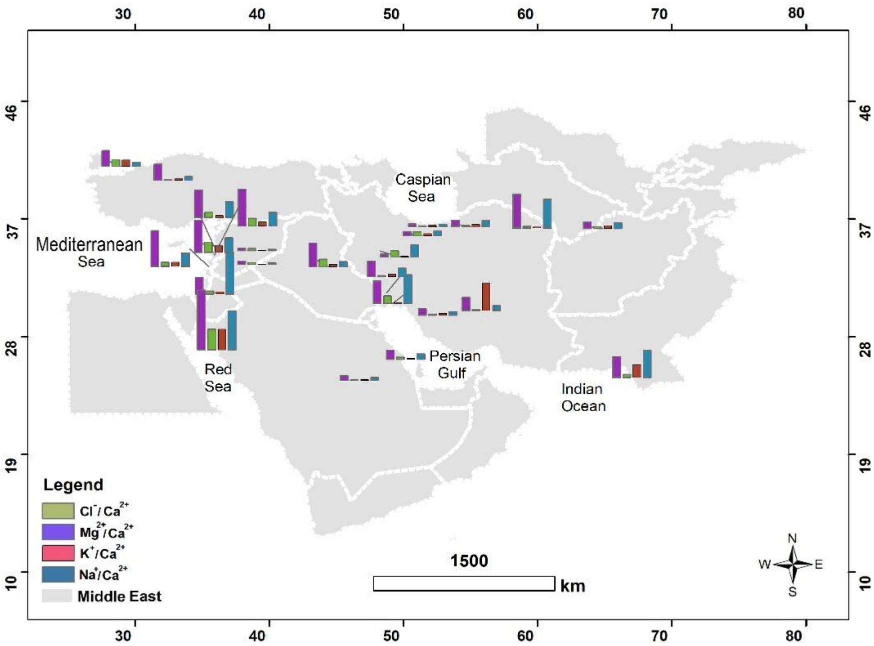

Figure 7. The distribution of major ion ratios in precipitation to Ca^{2+} in the studied stations.

4.2.1. The Sea Salt and Nonsea Salt Contributions to the Middle East Precipitation

To estimate the nonmarine and marine contributions of various ionic species to the Middle East precipitation, a nonsea salt fraction (NSSF) and sea salt fraction (SSF) were respectively calculated, and the results are presented in Table 1. The results demonstrate high NSS values for the Ca^{2+} and HCO_3^- ions at the studied stations due to the terrestrial origins of these ions. However, Cl^- shows much lower NSSF values than SSF values. In addition, the negative values of NSSF in some of the studied ions such as Cl^-, Mg^{2+}, and K^+ show mainly marine origins of these ions. The other ions in the precipitation samples of the studied stations show both marine and continental sources.

Table 1. The SSF and NSSF of the major ions in the Middle East precipitation.

Row	Station	Sea Salt Fraction (SSF)						Non Sea Salt Fraction (NSSF)					
		Ca^{2+}	K^+	Mg^{2+}	SO_4^{2-}	Cl^-	HCO_3^-	Ca^{2+}	K^+	Mg^{2+}	SO_4^{2-}	Cl^-	HCO_3^-
						Continental stations							
1	Shiraz	0.11	0.11	0.35	0.75	5.25	0.03	12.49	1.59	0.66	13.45	−0.15	0.33
2	Ahvaz	0.32	0.31	0.99	2.09	14.68	0.08	15.83	−0.31	−0.21	33.02	0.21	40.62
3	Shahroud	0.31	0.3	0.95	2.01	14.11	0.08	21.59	2.5	0.45	20.99	−6.11	44.12
4	Haraz	0.07	0.07	0.23	0.48	3.4	0.02	12.35	1.02	0.28	4.41	−1.21	43.79
5	Sarcheshmeh	0.06	0.06	0.2	0.42	2.93	0.02	5.68	9.29	0.18	19.39	1.56	5.01
6	Tehran	0.11	0.11	0.34	0.72	5.08	0.03	9.39	1.01	1.81	11.6	−2.61	23.02
7	Mashhad	0.94	0.91	2.92	6.15	43.3	0.25	12.82	−0.21	−1.46	19.87	−14.98	28.97
8	Arak	0.75	0.73	2.33	4.92	34.6	0.2	24.97	0.29	7.35	38.19	−30.17	62.27
9	Urmia	_	_	_	_	_	_	_	_	_	2.34	4.04	_
10	Riyadh	0.24	0.23	0.74	1.57	11.04	0.06	31.26	1.57	0.76	15.73	−1.54	−0.06
11	Eshidiya	0.15	0.15	0.47	0.99	6.96	0.04	1.47	1.81	1.53	8.24	−1.13	4.27
12	Ankara	0.48	0.46	1.48	3.13	22.04	0.13	52.42	4.97	1.43	116.97	29.72	146.27
13	Faryab	1.09	0.55	0.57	0.31	2.9	_	6.99	1.15	0.23	5.19	−0.10	_
14	Hadath	0.29	0.28	0.89	1.87	13.17	0.08	8.58	1.87	3.21	−0.79	6.71	34.09
15	Nabatieh	0.28	0.27	0.87	1.84	12.96	0.08	8.56	1.9	1.29	0.43	6.15	28.7
16	Palmyra	0.08	0.08	0.26	0.56	3.91	0.02	29.25	0.75	3.74	13.77	1.42	77.31
17	Damascus	0.06	0.06	0.2	0.42	2.93	0.02	22.94	0.44	1.8	19.33	1.57	45.73
18	Amman	0.56	0.54	1.74	3.66	25.79	0.15	5.07	0.33	−0.75	1.53	−20.06	10.95
19	Baghdad	2.5	1.24	1.29	0.71	6.61	_	17.95	2.57	7.11	51.9	19.59	_
20	Ramallah	0.43	0.42	1.34	2.82	19.85	0.11	−0.43	4.56	−1.34	−2.82	−19.85	−0.11
21	Jerdab	_	_	_	_	_	_	_	_	_	_	_	_
22	Tartus	0.32	0.31	0.99	2.08	14.66	0.08	8.08	0.79	1.81	3.12	−0.66	24.12
23	Dhahran	0.12	0.11	0.36	0.77	5.41	0.03	9.15	0.28	0.73	10.4	−0.33	4.45
24	Istanbul	0.07	0.06	0.21	0.43	3.06	0.02	7.11	2.65	2.73	8.97	3.88	−0.02
25	Tripoli	0.26	0.26	0.82	1.74	12.21	0.07	7.45	2.8	3.85	1.19	2.79	19.93
26	Damietta	_	_	_	_	_	_	_	_	_	143.54	37.13	_
27	Karachi	0.44	0.42	1.36	2.86	20.14	0.12	6.23	4.74	−0.18	16.21	−11.56	9.89
28	Mahshahr	0.92	0.89	2.85	6.01	42.27	0.24	12.61	−0.30	3.27	52.15	−23.95	33.83

4.2.2. Calculating the Enrichment Factor in the Middle East Precipitation

An enrichment factor (EF) was used to determine and examine the origins and contributions of the dominant ions in the Middle East precipitation [96,97]. The enrichment factor is calculated by comparing the elemental ratio between some major ions measured in the Middle East precipitation with a similar ratio in marine sources [98]. The calculated EF values show that the Ca^{2+}, $SO_4{}^{2-}$, and $HCO_3{}^{-}$ ions have terrestrial origins. However, the lower EF values for K^+, Cl^-, and Mg^{2+} show the important role of marine sources in these ions (Table 2).

Table 2. The enrichment factor (EF) of the major ions in the Middle East precipitation.

Row	Station	Ca^{2+}	K^+	Mg^{2+}	$SO_4{}^{2-}$	Cl^-	$HCO_3{}^-$
1	Shiraz	110.73	15.43	2.86	19.04	0.97	11.85
2	Ahvaz	50.75	–	0.79	16.84	1.01	479.04
3	Shahroud	71.56	9.45	1.47	11.47	0.57	540.91
4	Haraz	168.37	15.26	2.23	10.12	0.64	2224.4
5	Sarcheshmeh	90.3	151.88	1.91	47.55	1.53	296.38
6	Tehran	86.16	10.49	6.28	17.05	0.49	783
7	Mashhad	14.65	0.77	0.5	4.23	0.65	116.56
8	Arak	34.28	1.4	4.15	8.77	0.13	311.87
9	Urmia	–	–	–	–	–	–
10	Riyadh	131.61	7.77	2.02	11.03	0.86	–
11	Eshidiya	10.75	13.37	4.26	9.33	0.84	106.84
12	Ankara	110.69	11.73	1.96	38.35	2.35	1147.34
13	Faryab	64.69	22.01	1.41	17.6	0.96	–
14	Hadath	31.05	7.77	4.62	0.58	1.51	448.03
15	Nabatieh	31.47	7.98	2.47	1.23	1.47	383.68
16	Palmyra	346.06	10.11	15.19	25.8	1.36	3417.36
17	Damascus	361.83	8.12	10.13	47.41	1.54	2695.71
18	Amman	10.07	1.61	0.57	1.42	0.22	74.35
19	Baghdad	72.73	21.72	6.49	72.84	3.96	–
20	Ramallah	–	11.95	–	–	–	–
				Coastal stations			
21	Jerdab	–	–	–	–	–	–
22	Tartus	26.43	3.57	2.84	2.5	0.96	285.19
23	Dhahran	79.01	3.43	2.99	14.53	0.94	143.02
24	Istanbul	108.28	42.2	14.27	21.63	2.27	–
25	Tripoli	29.11	11.93	5.68	1.69	1.23	282.83
26	Damietta	–	–	–	–	–	–
27	Karachi	15.27	12.2	0.87	6.66	0.43	85.85
28	Mahshahr	14.76	0.66	2.15	9.68	0.43	139.22

4.2.3. The Acidity and Neutralizing Capacity of the Middle East Precipitation

The acidity of precipitation is normally affected by the existence of HNO_3, H_2SO_4, and organic acids in precipitation, while NH_3 and $CaCO_3$ in the environment neutralize the acidity of precipitation [80,99]. To test the acidity of precipitation after the neutralization process in the atmosphere, calculating fractional acidity (FA) using the equation $H^+/(SO_4{}^{2-}+NO_3{}^-)$ can provide valuable results. This index has been calculated and used in many previous studies [23,97,100]. In the studied stations, FA ranges from 0.0007 to 1.17 and has an average of 0.16. To study the relationship between acidity and neutralization more deeply, FA was plotted against pH (Figure 8). A strong positive correlation between FA and pH according to the coefficient of determination (R^2) value of 0.72 shows that $SO_4{}^{2-}$ and $NO_3{}^-$ are the main elements controlling the acidity of precipitation. Nevertheless, a large proportion of the species causing acidity are neutralized in the atmosphere [23].

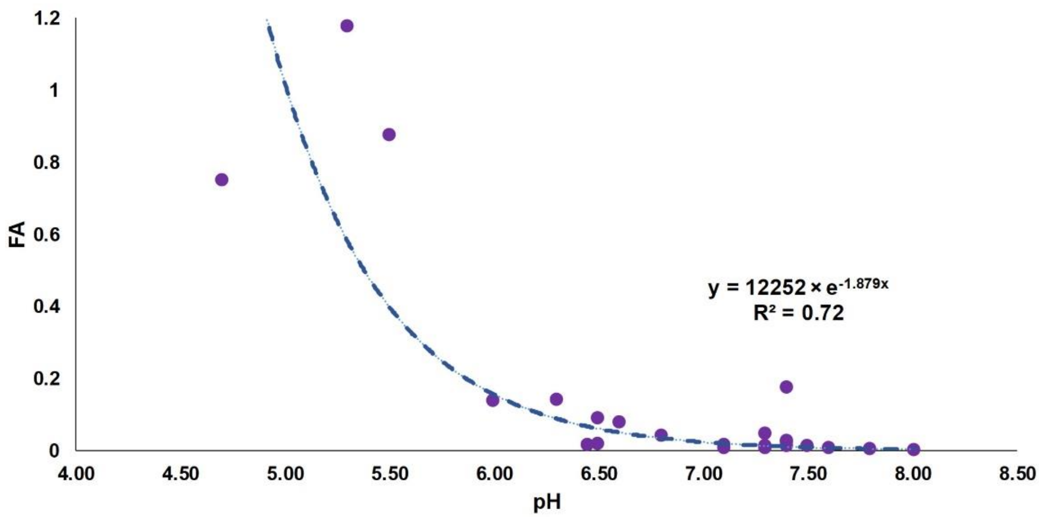

Figure 8. Regression analysis of FA and pH in the Middle East precipitation.

The neutralizing capacity of the major ions can also show the acidity potential of precipitation in the Middle East (Table 3). Calculating the neutralizing factor (NF) in the precipitation samples shows the following descending trend: Ca^{2+} (0.29) > Mg^{2+} (0.25) > K^+ (0.24). Therefore, Ca^{2+} is considered the major acid-neutralizing cation among the ions. This may be due to the terrestrial origin of this ion in controlling the chemistry of precipitation as well as the abundance of dust particles in the atmosphere of the Middle East. In most cases, the NF is much lower than unity, which confirms the fact that the acidic species have a more important role than the neutralizing ones. The NF is more than unity only at Baghdad station, where the neutralizing species are dominant.

Table 3. The NFs of the major ions in the Middle East precipitation.

Row	Station	Ca^{2+}	K^+	Mg^{2+}
			Continental stations	
1	Shiraz	–	–	–
2	Ahvaz	–	–	–
3	Shahroud	–	–	–
4	Haraz	0.013	0.042	0.013
5	Sarcheshmeh	0.045	0.152	0.045
6	Tehran	0.016	0.048	0.016
7	Mashhad	0.952	0.047	1.61
8	Arak	0.665	0.025	1.115
9	Urmia	–	–	–
10	Riyadh	0.153	0.471	0.146
11	Eshidiya	0.084	0.263	0.084
12	Ankara	0.003	0.011	0.003
13	Faryab	0.286	0.15	0.144
14	Hadath	0.061	0.187	0.059
15	Nabatieh	0.036	0.111	0.034
16	Palmyra	0.007	0.024	0.007
17	Damascus	0.007	0.023	0.007
18	Amman	0.087	0.269	0.084
19	Baghdad	3.521	1.817	1.746
20	Ramallah	0.02	0.062	0.019
			Coastal stations	
21	Jerdab	–	–	–
22	Tartus	0.032	0.098	0.031
23	Dhahran	0.012	0.037	0.011
24	Istanbul	0.163	0.488	0.14
25	Tripoli	0.059	0.185	0.059
26	Damietta	–	–	–
27	Karachi	0.154	0.476	0.147
28	Mahshahr	0.089	0.276	0.086

Finally, the relative contributions of nitric and sulfuric acids (the main acidic elements in precipitation) to the Middle East precipitation were studied using some ion ratios. Firstly, the SO_4^{2-}/NO_3^- ratio in precipitation ranges from 0.38 to 22.0, with an average of 3.76. This demonstrates that sulfuric acid has a stronger role in the acidity of precipitation than nitric acid. Secondly, the $(NO_3^- + Cl^-)/(SO_4^{2-})$ ratio was studied in precipitation. This ratio ranges from 0.27 to 20.73, with an average of 3.35. At some of the stations, including Haraz, Urmia, Tripoli, Hadath, Nabatieh, Tartus, Palmyra, Amman, Dhahran, Ankara, and Faryab, the $(NO_3^- + Cl^-)/(SO_4^{2-})$ ratio shows values higher than unity. However, the $(NO_3^- + Cl^-)/(SO_4^{2-})$ ratio at Mahshahr, Sarcheshmeh, Tehran, Damietta, Damascus, and Eshidiya stations shows values lower than unity. At the stations with a $(NO_3^- + Cl^-)/(SO_4^{2-})$ ratio lower than unity, the role of sulfuric acid is more dominant. However, at the stations with a $(NO_3^- + Cl^-)/(SO_4^{2-})$ ratio more than unity, the role of hydrochloric and nitric acids in the acidity of water is significant.

On the other hand, comparing the NH_4^+/NO_3^- ratios at a few stations in the Middle East (NH_4^+ was analyzed at a few stations) shows that ammonium (NH_4^+) cannot neutralize the acidic N-containing species in the Middle East precipitation. This is because the NH_4^+/NO_3^- ratio is lower than unity in most cases and ranges from 0.07 to 5, with an average of 0.77. The high value of the NH_4^+/NO_3^- ratio (~5) at Eshidiya station is due to the significant amount of ammonium produced by chemical manufacturing industries in this area. A high amount of ammonium completely neutralizes N-containing acidic compounds and possibly forms NH_4NO_3 in the atmosphere [101].

4.3. Applying Statistical and Machine Learning Techniques in Hydrochemical Studies of the Middle East Precipitation

To study the sources of ions in the Middle East precipitation more deeply, statistical techniques such as PCA were applied (Text Code S2). The varimax rotation of the PCA, which covers more than 71% of the total variance, is depicted in Table 4. The first factor has a high loading for Ca^{2+}, HCO_3^-, Cl^-, SO_4^{2-}, EC, and TDS, which explains 52% of the total variance. This factor shows the main role of the ions with terrestrial origins in precipitation. They mainly originate from the dissolution of carbonate-containing (such as calcite, dolomite, and aragonite) and/or evaporative minerals (such as gypsum, anhydrite, and hydrophilite). The second factor, which covers 19.0% of the total variance, has a significant loading for Mg^{2+}, Na^+, K^+, and pH. The second factor shows the importance of the concentrations of some ions and their correlation with the pH/acidity of precipitation. The K^+ ion mainly originates from terrestrial sources and is inversely correlated with pH. However, Mg^{2+} and Na^+ have a mainly marine origin and are directly correlated with pH.

Table 4. The PCA varimax rotation of hydrochemical parameters of the Middle East precipitation.

Element	Component	
	1	2
Ca^{2+}	0.85	−0.04
Mg^{2+}	0.34	−0.61
Na^+	0.43	−0.57
K^+	0.23	0.72
SO_4^{2-}	0.94	0.03
HCO_3^-	0.88	−0.06
Cl^-	0.82	−0.01
pH	−0.21	−0.81
EC	0.96	0.1
TDS	0.87	0.084

In addition to statistical techniques, machine learning algorithms were also used to simulate the TDS values in precipitation. Various machine learning algorithms, including ANN, DNN, decision tree, and gradient boosting (Gboost), were also applied to the precipitation data to simulate the TDS values. First, the importance percentage of each major ion affecting the TDS values in precipitation was determined (Figure 9). Studying the importance percentage of various ions controlling the TDS values in precipitation by different machine learning algorithms shows that Ca^{2+} and Na^{+} are the main ions controlling the TDS values in precipitation according to the Gboost and DNN models. The Cl^{-} and HCO_3^{-} ions were the major ions controlling the TDS values in precipitation in the ANN model, as are SO_4^{2-} and Cl^{-} in the decision tree model. Among the cations, Ca^{2+} mainly originates from terrestrial sources, while Na^{+} mainly originates from marine sources. Among the anions, Cl^{-} and SO_4^{2-} have mainly marine origins, while HCO_3^{-} mainly originates from terrestrial sources.

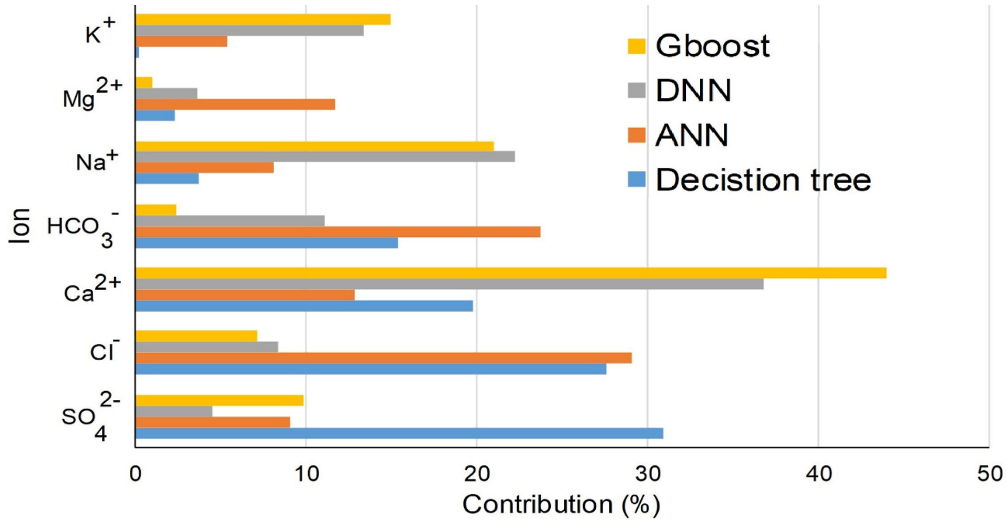

Figure 9. The percentage importance of different major ions in the Middle East precipitation (obtained from various machine learning models).

Furthermore, as an indicator of the hydrochemistry of precipitation, TDS was simulated by these machine learning algorithms. Then, the accuracy of the developed models was validated by R^2 values (Table 5).

Table 5. The validation of the developed models in simulating the TDS values in precipitation based on R^2 values.

Method		DNN	ANN	Decision Tree	Gradient Boosting (Gboost)
Train set	R^2	0.49	0.59	0.64	0.71
Test set	R^2	0.45	0.52	0.51	0.67

It can be observed that among the studied machine learning algorithms, gradient boosting (Gboost) has the highest R^2 values both in the train and test sets. This confirms the higher accuracy of the model developed by Gboost compared with those developed by other machine learning methods. Normally, boosting machine learning algorithms, such as gradient boosting (Gboost), extra gradient boosting (XGboost), Ada boosting, and cat boosting, improve weak regression or decision tree models to obtain more accurate machine learning models. This is why the model developed by Gboost is more accurate and shows higher R^2 values.

5. Conclusions

The hydrochemical analyses showed that the particles originating from terrestrial sources controlled the quality of precipitation across the Middle East. This was due to the significant amount of dust particles in the atmosphere of the Middle East originating from dry and bare lands. The dust particles originating from evaporative and carbonate minerals were the main sources affecting precipitation. In addition, marine and anthropogenic sources also had a minor effect on the quality of precipitation in this region. Precipitation in some of the stations had an acidic nature, while it had a nonacidic or neutralized nature in some other stations. $SO_4{}^{2-}$ and $NO_3{}^{-}$ were the main ions controlling the acidity of precipitation. On the other hand, the major acid-neutralizing cation in the Middle East precipitation was Ca^{2+}. Finally, studying the importance percentages of various ions in controlling the TDS values in precipitation and simulating the TDS values using machine learning algorithms (DNN and Gboost models) showed that Ca^{2+} and Na^{+} were the dominant ions controlling the TDS values in precipitation. Cl^{-} and $HCO_3{}^{-}$ were the main ions in the ANN model, whereas $SO_4{}^{2-}$ and Cl^{-} were the major ions in the decision tree model. The validation of the developed models showed that Gboost was the most accurate model in simulating the TDS values in precipitation due to its higher R^2 values in both the train and test sets.

Supplementary Materials: The following supporting information can be downloaded at: https://www.mdpi.com/article/10.3390/w14172657/s1, Table S1: The ratio of ions to Na^{+} and Ca^{2+}, as well as the $SO_4{}^{2-}/NO_3{}^{-}$ ratio in precipitation at the studied stations, Text Code S2: code for PCA of precipitation data in the studied stations across the Middle East.

Author Contributions: Conceptualization, M.H., H.G.M. and M.M.; methodology, L.G.; software, M.H.; validation, M.H., M.M. and S.A.; formal analysis, M.H. and H.G.M.; investigation, M.H.; resources, M.H. and M.M.; data curation, M.H.; writing—original draft preparation, M.H.; visualization, S.A.; supervision, L.G.; project administration, L.G. All authors have read and agreed to the published version of the manuscript.

Funding: This research received no external funding.

Data Availability Statement: The data of this study are available from the first author [M.H.] upon reasonable request.

Acknowledgments: The first author acknowledges the postdoctoral fellowship (no. MU-PD-2021-13) from the Faculty of Environment and Resource Studies, Mahidol University. The authors also express their gratitude to their colleagues at Mahidol University in Thailand and Vigo University (Ourense campus) in Spain for their support during this study.

Conflicts of Interest: The authors declare no conflict of interest.

References

1. Bozorg-Haddad, O.; Zolghadr-Asli, B.; Sarzaeim, P.; Aboutalebi, M.; Chu, X.; Loáiciga, H.A. Evaluation of water shortage crisis in the Middle East and possible remedies. *J. Water Supply Res. Technol.* **2019**, *69*, 85–98. [CrossRef]
2. Baconi, T. Testing the Water: How Water Scarcity Could Destabilise the Middle East and North Africa. 2018. Available online: https://ecfr.eu/publication/how_water_scarcity_could_destabilise_the_middle_east_and_north_africa/ (accessed on 11 July 2022).
3. Araghi, A.; Mousavi-Baygi, M.; Adamowski, J.; Martinez, C. Association between three prominent climatic teleconnections and precipitation in Iran using wavelet coherence. *Int. J. Clim.* **2016**, *37*, 2809–2830. [CrossRef]
4. Balling, R.C.; Kiany, M.S.K.; Roy, S.S.; Khoshhal, J. Trends in Extreme Precipitation Indices in Iran: 1951–2007. *Adv. Meteorol.* **2016**, *2016*, 1–8. [CrossRef]
5. Rahimzadeh, F.; Asgari, A.; Fattahi, E. Variability of extreme temperature and precipitation in Iran during recent decades. *Int. J. Clim.* **2008**, *29*, 329–343. [CrossRef]
6. Pourasghar, F.; Tozuka, T.; Jahanbakhsh, S.; Sarraf, B.S.; Ghaemi, H.; Yamagata, T. The interannual precipitation variability in the southern part of Iran as linked to large-scale climate modes. *Clim. Dyn.* **2012**, *39*, 2329–2341. [CrossRef]
7. Khalili, A.; Rahimi, J. High-resolution spatiotemporal distribution of precipitation in Iran: A comparative study with three global-precipitation datasets. *Arch. Meteorol. Geophys. Bioclimatol. Ser. B* **2013**, *118*, 211–221. [CrossRef]
8. Javari, M. Trend and Homogeneity Analysis of Precipitation in Iran. *Climate* **2016**, *4*, 44. [CrossRef]
9. Raziei, T.; Mofidi, A.; dos Santos, J.C.A.; Bordi, I. Spatial patterns and regimes of daily precipitation in Iran in relation to large-scale atmospheric circulation. *Int. J. Clim.* **2011**, *32*, 1226–1237. [CrossRef]
10. Al-Khashman, O.A. Ionic composition of wet precipitation in the Petra Region, Jordan. *Atmos. Res.* **2005**, *78*, 1–12. [CrossRef]
11. Salameh, E.; Rimawi, O. Hydrochemistry of precipitation of northern Jordan. *Int. J. Environ. Stud.* **1988**, *32*, 203–216. [CrossRef]

12. Shamsi, A.; Karami, G.; Taheri, A.; Hunkeler, D. Hydrochemistry and stable isotopes study of the precipitation at Haraz Basin, north of Iran. *Geopersia* **2019**, *10*, 23–39. [CrossRef]
13. Zhai, Y.; Wang, J.; Zhang, Y.; Teng, Y.; Zuo, R.; Huan, H. Hydrochemical and isotopic investigation of atmospheric precipitation in Beijing, China. *Sci. Total Environ.* **2013**, *456–457*, 202–211. [CrossRef] [PubMed]
14. Saeedi, M.; Pajooheshfar, S.P. Acid Rain Examination and Chemical Composition of Atmospheric Precipitation in Tehran, Iran. *Environ. Asia* **2012**, *5*, 39–47. [CrossRef]
15. Okuda, T.; Iwase, T.; Ueda, H.; Suda, Y.; Tanaka, S.; Dokiya, Y.; Fushimi, K.; Hosoe, M. Long-term trend of chemical constituents in precipitation in Tokyo metropolitan area, Japan, from 1990 to 2002. *Sci. Total Environ.* **2005**, *339*, 127–141. [CrossRef] [PubMed]
16. Vong, R.J.; Larson, T.V.; Covert, D.S.; Waggoner, A.P. Measurement and modeling of Western Washington precipitation chemistry. *Water Air Soil Pollut.* **1985**, *26*, 71–84. [CrossRef]
17. De Mello, W. Precipitation chemistry in the coast of the Metropolitan Region of Rio de Janeiro, Brazil. *Environ. Pollut.* **2001**, *114*, 235–242. [CrossRef]
18. Ayers, G.P.; Gillett, R.W. Some observations on the acidity and composition of rainwater in Sydney, Australia, during the summer of 1980?81. *J. Atmos. Chem.* **1984**, *2*, 25–46. [CrossRef]
19. Ali, K.; Momin, G.; Tiwari, S.; Safai, P.; Chate, D.; Rao, P. Fog and precipitation chemistry at Delhi, North India. *Atmos. Environ.* **2004**, *38*, 4215–4222. [CrossRef]
20. Miller, N.H. The Composition of Rain-Water Collected in the Hebrides in Iceland; With Special Reference to Theamount of Nitrogen as Ammonia and as Nitrates. *Scott. Met. Soc.* **1913**, *16*, 141–158. Available online: https://repository.rothamsted.ac.uk/item/97w54/the-composition-of-rainwater-collected-in-the-hebrides-in-iceland-with-special-reference-to-the-amount-of-nitrogen-as-ammonia-and-as-nitrates (accessed on 11 July 2022).
21. Schemenauer, R.S.; Cereceda, P. Monsoon cloudwater chemistry on the Arabian Peninsula. *Atmos. Environ. Part. A Gen. Top.* **1992**, *26*, 1583–1587. [CrossRef]
22. Kattan, Z. Chemical and environmental isotope study of precipitation in Syria. *J. Arid Environ.* **1997**, *35*, 601–615. [CrossRef]
23. Keresztesi, Á.; Birsan, M.-V.; Nita, I.-A.; Bodor, Z.; Szép, R. Assessing the neutralisation, wet deposition and source contributions of the precipitation chemistry over Europe during 2000–2017. *Environ. Sci. Eur.* **2019**, *31*, 50. [CrossRef]
24. Abdemanafi, D.; Meshkatee, A.-H.; Hajjam, S.; Vazifedoust, M. The study of relation between aerosols and quality of rain water over Tehran during 2012–2013 years. *J. Environ. Sci. Tech.* **2017**, *19*, 15–30.
25. Saad, Z.; Slim, K.; Ghaddar, A.; Nasreddine, M.; Kattan, Z. Chemical composition of rain water in Lebanon. *J. Eur. Hydrol.* **2000**, *31*, 223–238. [CrossRef]
26. Naimabadi, A.; Shirmardi, M.; Maleki, H.; Teymouri, P.; Goudarzi, G.; Shahsavani, A.; Sorooshian, A.; Babaei, A.A.; Mehrabi, N.; Baneshi, M.M.; et al. On the chemical nature of precipitation in a populated Middle Eastern Region (Ahvaz, Iran) with diverse sources. *Ecotoxicol. Environ. Saf.* **2018**, *163*, 558–566. [CrossRef] [PubMed]
27. Alkhashman, O. Study of chemical composition in wet atmospheric precipitation in Eshidiya area, Jordan. *Atmos. Environ.* **2005**, *39*, 6175–6183. [CrossRef]
28. Ghadimi, F.; Ghomi, M.; Ranjbar, M.; Hajati, A. Sources of contamination in rainwater by major and heavy elements in Arak, Iran. *J. Water Sci. Res.* **2013**, *5*, 67–84.
29. Fabbian, D.; de Dear, R.; Lellyett, S.C. Application of Artificial Neural Network Forecasts to Predict Fog at Canberra International Airport. *Weather Forecast* **2007**, *22*, 372–381. [CrossRef]
30. Rumelhart, D.E.; Hinton, G.E.; McClelland, J.L. A general framework for Parallel Distributed Processing. In *Parallel Distributed Processing*; The MIT Press: Cambridge, MA, USA, 1986; p. 517.
31. Hall, T.; Brooks, H.E.; Doswell, C.A., III. Precipitation Forecasting Using a Neural Network. *Weather Forecast* **1999**, *14*, 338–345. [CrossRef]
32. Mislan; Haviluddin; Hardwinarto, S.; Sumaryono; Aipassa, M. Rainfall Monthly Prediction Based on Artificial Neural Network: A Case Study in Tenggarong Station, East Kalimantan—Indonesia. *Procedia Comput. Sci.* **2015**, *59*, 142–151. [CrossRef]
33. Moustris, K.P.; Larissi, I.K.; Nastos, P.T.; Paliatsos, A.G. Precipitation Forecast Using Artificial Neural Networks in Specific Regions of Greece. *Water Resour. Manag.* **2011**, *25*, 1979–1993. [CrossRef]
34. Kang, J.; Wang, H.; Yuan, F.; Wang, Z.; Huang, J.; Qiu, T. Prediction of Precipitation Based on Recurrent Neural Networks in Jingdezhen, Jiangxi Province, China. *Atmosphere* **2020**, *11*, 246. [CrossRef]
35. Ogunrinde, A.T.; Oguntunde, P.G.; Fasinmirin, J.T.; Akinwumiju, A.S. Application of artificial neural network for forecasting standardized precipitation and evapotranspiration index: A case study of Nigeria. *Eng. Rep.* **2020**, *2*. [CrossRef]
36. Bączkiewicz, A.; Wątróbski, J.; Sałabun, W.; Kołodziejczyk, J. An ANN Model Trained on Regional Data in the Prediction of Particular Weather Conditions. *Appl. Sci.* **2021**, *11*, 4757. [CrossRef]
37. Zabbah, I.; Roshani, A.R.; Khafage, A. Prediction of monthly rainfall using artificial neural network mixture approach, Case Study: Torbat-e Heydariyeh. *J. Earth Space Phys.* **2018**, *44*, 115–126. [CrossRef]
38. Yen, M.-H.; Liu, D.-W.; Hsin, Y.-C.; Lin, C.-E.; Chen, C.-C. Application of the deep learning for the prediction of rainfall in Southern Taiwan. *Sci. Rep.* **2019**, *9*, 12774. [CrossRef]
39. Weesakul, U.; Chaiyasarn, K.; Mahat, S. Long-term rainfall forecasting using deep neural network coupling with input variables selection technique: A case study of Ping River Basin, Thailand. Eng. *Appl. Sci. Res.* **2021**, *48*, 209–220.

40. Das, S.; Chakraborty, R.; Maitra, A. A random forest algorithm for nowcasting of intense precipitation events. *Adv. Space Res.* **2017**, *60*, 1271–1282. [CrossRef]
41. Wolfensberger, D.; Gabella, M.; Boscacci, M.; Germann, U.; Berne, A. RainForest: A random forest algorithm for quantitative precipitation estimation over Switzerland. *Atmos. Meas. Tech.* **2021**, *14*, 3169–3193. [CrossRef]
42. Ortiz-García, E.G.; Salcedo-Sanz, S.; Casanova-Mateo, C. Accurate precipitation prediction with support vector classifiers: A study including novel predictive variables and observational data. *Atmos. Res.* **2014**, *139*, 128–136. [CrossRef]
43. Du, J.; Liu, Y.; Yu, Y.; Yan, W. A Prediction of Precipitation Data Based on Support Vector Machine and Particle Swarm Optimization (PSO-SVM) Algorithms. *Algorithms* **2017**, *10*, 57. [CrossRef]
44. Zhang, J.; Yao, Y.; Cao, N. Prediction of whether precipitation based on decision tree. *J. Geomat.* **2017**, *42*, 107–109. [CrossRef]
45. Monego, V.S.; Anochi, J.A.; Velho, H.F.D.C. South America Seasonal Precipitation Prediction by Gradient-Boosting Machine-Learning Approach. *Atmosphere* **2022**, *13*, 243. [CrossRef]
46. Beck, H.E.; Zimmermann, N.E.; McVicar, T.R.; Vergopolan, N.; Berg, A.; Wood, E.F. Present and future Köppen-Geiger climate classification maps at 1-km resolution. *Sci. Data.* **2018**, *5*, 180214. [CrossRef]
47. Mohebi, A. Studying the parameters influenceing precipitation variations across Middle East. *Water Resour.* **2012**, *15*, 205–209.
48. Heydarizad, M.; Gimeno, L.; Sorí, R.; Minaei, F.; Mayvan, J.E. The Stable Isotope Characteristics of Precipitation in the Middle East Highlighting the Link between the Köppen Climate Classifications and the $\delta^{18}O$ and $\delta^{2}H$ Values of Precipitation. *Water* **2021**, *13*, 2397. [CrossRef]
49. Alijani, B. *Iran Climatology*, 5th ed.; Payam Nour Publication: Tehran, Iran, 2000; p. 230.
50. Drumond, A.; Taboada, E.; Nieto, R.; Gimeno, L.; Vicente-Serrano, S.M.; Ignacio López-Moreno, J. Lagrangian analysis of the present-day sources of moisture for major ice-core sites. *Earth Syst. Dynam.* **2016**, *7*, 549–558. [CrossRef]
51. Heydarizad, M. Meteoric Water Lines of Iran for Various Precipitation Sources. Ph.D. Thesis, Shiraz University, Shiraz, Iran, 2018.
52. Heydarizad, M.; Raeisi, E.; Sori, R.; Gimeno, L. The Identification of Iran's Moisture Sources Using a Lagrangian Particle Dispersion Model. *Atmosphere* **2018**, *9*, 408. [CrossRef]
53. Dee, D.P.; Uppala, S.M.; Simmons, A.J.; Berrisford, P.; Poli, P.; Kobayashi, S.; Andrae, U.; Balmaseda, M.A.; Balsamo, G.; Bauer, P.; et al. The ERA-Interim reanalysis: Configuration and performance of the data assimilation system. *Q. J. R. Meteorol. Soc.* **2011**, *137*, 553–597. [CrossRef]
54. Moore, F.; Attar, A. Rainwater and the resulting runoff chemistry in Shiraz city, southwest Iran. *Int. J. Environ. Stud.* **2011**, *68*, 703–717. [CrossRef]
55. Mehr, M.R.; Keshavarzi, B.; Sorooshian, A. Influence of natural and urban emissions on rainwater chemistry at a southwestern Iran coastal site. *Sci. Total Environ.* **2019**, *668*, 1213–1221. [CrossRef] [PubMed]
56. Mirhosseini, M.; Shahabpour, J.; Behrouz, M. Hydrochemical charcterstic of acidic rain in Sarcheshmeh area in Kerman province. *Scinece J.* **2008**, *19*, 74–83.
57. Behravesh, F.; Mahmoudi Gharaee, M.H.; Ghasem zadeh, F.; Avaz Moghadam, S. Quality assessment of precipitation and run off in Mashhad city. In Proceedings of the the 2nd Iranian Rainwater Catchment Systems Association; Iranian Rainwater Catchment Systems Association: Mashhad, Iran, 2019; pp. 1–9.
58. Kazemi, G.A.; Ichiyanagi, K.; Shimada, J. Isotopic characteristics, chemical composition and salinization of atmospheric precipitation in Shahrood, northeastern Iran. *Environ. Earth Sci.* **2014**, *73*, 361–374. [CrossRef]
59. Hajizadeh, Y.; Nemati, S.; Aghapour, A.A.; Abdolahnejad, A.; Mohammadi, A.; Panahi, H.; Moghanjooghi, S.M.; Nikoonahad, A. Influence of Air Pollution on Chemical Quality of Wet Atmospheric Deposition: A Case Study in Urmia, Iran. *Iran. J. Heal. Saf. Environ.* **2017**, *5*, 904–910. Available online: https://www.researchgate.net/publication/320629105_Influence_of_Air_Pollution_on_Chemical_Quality_of_Wet_Atmospheric_Deposition_a_Case_Study_in_Urmia_Iran (accessed on 11 July 2022).
60. Michelsen, N.; Reshid, M.; Siebert, C.; Schulz, S.; Knöller, K.; Weise, S.M.; Rausch, R.; Al-Saud, M.; Schüth, C. Isotopic and chemical composition of precipitation in Riyadh, Saudi Arabia. *Chem. Geol.* **2015**, *413*, 51–62. [CrossRef]
61. Precipitation Quality and Related Atmospheric Chemistry over the Greater Damietta Area-Egypt. *Res. J. Environ. Sci.* **2008**, *2*, 252–265. [CrossRef]
62. Masood, S.S.; Saied, S.; Siddique, A.; Mohiuddin, S.; Hussain, M.M.; Khan, M.K.; Khwaja, H.A. nfluence of urban–coastal activities on organic acids and major ionchemistry of wet precipitation at a metropolis in Pakistan. *Arab. J. Geosci.* **2018**, *11*, 802. [CrossRef]
63. Ghanem, M.; Shalash, I.; Al-Rimmawi, H. Hydrochemical Characteristics of Rainwater in Ramallah District. *Asian J. Earth Sci.* **2010**, *3*, 11–19. [CrossRef]
64. Al Charideh, A.R.; Zakhem, B.A. Distribution of tritium and stable isotopes in precipitation in Syria. *Hydrol. Sci. J.* **2010**, *55*, 832–843. [CrossRef]
65. Ghaleb, N.; Salman, A.; Qassim, S.; Ebrahim, A.; Saleh, M. Quality Assessment of Rainwater from Rainwater Harvesting Systems in Jerdab, Kingdom of Bahrain. *Int. J. Eng. Adv. Res. Technol.* **2018**, *4*, 1–4.
66. Topçu, S.; Incecik, S.; Atimtay, A.T. Chemical composition of rainwater at EMEP station in Ankara, Turkey. *Atmos. Res.* **2002**, *65*, 77–92. [CrossRef]
67. Başak, B.; Alagha, O. The chemical composition of rainwater over Büyükçekmece Lake, Istanbul. *Atmos. Res.* **2004**, *71*, 275–288. [CrossRef]
68. AL-Adili, A.; Sadeq, J. Hydrochemical study of rain water in Baghdad city, Iraq. *Eng. Tech.* **2008**, *26*, 408.

69. Banks, D. A Hydrogeological Atlas of Faryab Province, Northern Afghanistan. 2014. Available online: https://eprints.gla.ac.uk/107735/ (accessed on 11 July 2022).
70. Al-Momani, I. Trace elements in atmospheric precipitation at Northern Jordan measured by ICP-MS: Acidity and possible sources. *Atmos. Environ.* **2003**, *37*, 4507–4515. [CrossRef]
71. Kulshrestha, U.; Sarkar, A.; Srivastava, S.; Parashar, D. Investigation into atmospheric deposition through precipitation studies at New Delhi (India). *Atmos. Environ.* **1996**, *30*, 4149–4154. [CrossRef]
72. Arsene, C.; Olariu, R.I.; Mihalopoulos, N. Chemical composition of rainwater in the northeastern Romania, Iasi region (2003–2006). *Atmos. Environ.* **2007**, *41*, 9452–9467. [CrossRef]
73. Rao, P.; Tiwari, S.; Matwale, J.; Pervez, S.; Tunved, P.; Safai, P.; Srivastava, A.; Bisht, D.; Singh, S.; Hopke, P. Sources of chemical species in rainwater during monsoon and non-monsoonal periods over two mega cities in India and dominant source region of secondary aerosols. *Atmos. Environ.* **2016**, *146*, 90–99. [CrossRef]
74. Kulshrestha, U.; Kulshrestha, M.J.; Sekar, R.; Sastry, G.; Vairamani, M. Chemical characteristics of rainwater at an urban site of south-central India. *Atmos. Environ.* **2003**, *37*, 3019–3026. [CrossRef]
75. Chen, H.-Y.; Hsu, L.-F.; Huang, S.-Z.; Zheng, L. Assessment of the Components and Sources of Acid Deposition in Northeast Asia: A Case Study of the Coastal and Metropolitan Cities in Northern Taiwan. *Atmosphere* **2020**, *11*, 983. [CrossRef]
76. Bisht, D.S.; Srivastava, A.; Joshi, H.; Ram, K.; Singh, N.; Naja, M.; Tiwari, S. Chemical characterization of rainwater at a high-altitude site "Nainital" in the central Himalayas, India. *Environ. Sci. Pollut. Res.* **2016**, *24*, 3959–3969. [CrossRef]
77. Anatolaki, C.; Tsitouridou, R. Relationship between acidity and ionic composition of wet precipitation: A two years study at an urban site, Thessaloniki, Greece. *Atmos. Res.* **2009**, *92*, 100–113. [CrossRef]
78. Jolliffe, I.T.; Cadima, J. Principal component analysis: A review and recent developments. *Philos. Trans. R. Soc. A Math. Phys. Eng. Sci.* **2016**, *374*, 20150202. [CrossRef] [PubMed]
79. R Core Team R: A Language and Environment for Statistical Computing. 2018. Available online: https://www.gbif.org/tool/81287/r-a-language-and-environment-for-statistical-computing (accessed on 11 July 2022).
80. Xu, Z.; Wu, Y.; Liu, W.-J.; Liang, C.-S.; Ji, J.; Zhao, T.; Zhang, X. Chemical composition of rainwater and the acid neutralizing effect at Beijing and Chizhou city, China. *Atmos. Res.* **2015**, *164–165*, 278–285. [CrossRef]
81. Huang, K.; Zhuang, G.; Xu, C.; Wang, Y.; Tang, A. The chemistry of the severe acidic precipitation in Shanghai, China. *Atmos. Res.* **2008**, *89*, 149–160. [CrossRef]
82. Tiwari, S.; Hopke, P.K.; Thimmaiah, D.; Dumka, U.C.; Srivastava, A.K.; Bisht, D.S.; Rao, P.S.; Chate, D.M.; Srivastava, M.K.; Tripathi, S.N. Nature and Sources of Ionic Species in Precipitation across the Indo-Gangetic Plains, India. *Aerosol Air Qual. Res.* **2016**, *16*, 943–957. [CrossRef]
83. Sahin, M.; Incecik, S.; Topcu, S.; Yildirim, A. Analysis of Atmospheric Conditions during Air Pollution Episodes in Ankara, Turkey. *J. Air Waste Manag. Assoc.* **2001**, *51*, 972–982. [CrossRef]
84. Ali-Mohamed, A.Y. Estimation of inorganic particulate matter in the atmosphere of Isa Town, Bahrain, by dry deposition. *Atmos. Environ. Part. B Urban. Atmos.* **1991**, *25*, 397–405. [CrossRef]
85. Ali-Mohamed, A. Estimation of inorganic particulate matter in atmospheres of villages in Bahrain, by dry fall. *Atmos. Environ.* **1995**, *29*, 1519–1529. [CrossRef]
86. Madany, I.M.; Akhter, M.S.; Al Jowder, O. The correlations between heavy metals in residential indoor dust and outdoor street dust in Bahrain. *Environ. Int.* **1994**, *20*, 483–492. [CrossRef]
87. Mohammadzadeh, H.; Heydarizad, M. A conceptual model for water resources circulation patterns in Andarokh-Kardeh region (NE, Iran). *Geochemistry* **2020**, *80*, 125593. [CrossRef]
88. Ayati, F.; Yavuz, F.; Noghreyan, M.; Haroni, H.A.; Yavuz, R. Chemical characteristics and composition of hydrothermal biotite from the Dalli porphyry copper prospect, Arak, central province of Iran. *Miner. Pet.* **2008**, *94*, 107–122. [CrossRef]
89. Anil, I.; Alagha, O.; Blaisi, N.I.; Mohamed, I.A.; Barghouthi, M.H.; Manzar, M.S. Source Identification of Episodic Rain Pollutants by New Approach: Combining Satellite Observations and Backward Air Mass Trajectories. *Aerosol Air Qual. Res.* **2019**, *9*, 2827–2843. [CrossRef]
90. Négrel, P.; Roy, S. Chemistry of rainwater in the Massif Central (France): A strontium isotope and major element study. *Appl. Geochem.* **1998**, *13*, 941–952. [CrossRef]
91. Kattan, Z. Factors affecting the chemical composition of precipitation in Syria. *Environ. Sci. Pollut. Res.* **2020**, *27*, 28408–28428. [CrossRef]
92. Lu, X.; Li, L.Y.; Li, N.; Yang, G.; Luo, D.; Chen, J. Chemical characteristics of spring rainwater of Xi'an city, NW China. *Atmos. Environ.* **2011**, *45*, 5058–5063. [CrossRef]
93. Wang, Y.; Zhuang, G.; Zhang, X.; Huang, K.; Xu, C.; Tang, A.; Chen, J.; An, Z. The ion chemistry, seasonal cycle, and sources of PM2.5 and TSP aerosol in Shanghai. *Atmos. Environ.* **2006**, *40*, 2935–2952. [CrossRef]
94. Vet, R.; Artz, R.S.; Carou, S.; Shaw, M.; Ro, C.-U.; Aas, W.; Baker, A.; Bowersox, V.C.; Dentener, F.; Galy-Lacaux, C.; et al. A global assessment of precipitation chemistry and deposition of sulfur, nitrogen, sea salt, base cations, organic acids, acidity and pH, and phosphorus. *Atmos. Environ.* **2014**, *93*, 3–100. [CrossRef]
95. Tuncer, B.; Bayar, B.; Yeşilyurt, C.; Tuncel, G. Ionic composition of precipitation at the Central Anatolia (Turkey). *Atmos. Environ.* **2001**, *35*, 5989–6002. [CrossRef]

96. Yatkin, S.; Adali, M.; Bayram, A. A study on the precipitation in Izmir, Turkey: Chemical composition and source apportionment by receptor models. *J. Atmos. Chem.* **2015**, *73*, 241–259. [CrossRef]
97. Szép, R.; Bodor, Z.; Miklóssy, I.; Nita, I.-A.; Oprea, O.A.; Keresztesi, A. Influence of peat fires on the rainwater chemistry in intra-mountain basins with specific atmospheric circulations (Eastern Carpathians, Romania). *Sci. Total Environ.* **2018**, *647*, 275–289. [CrossRef]
98. Xiao, J. Chemical composition and source identification of rainwater constituents at an urban site in Xi'an. *Environ. Earth Sci.* **2016**, *75*, 209. [CrossRef]
99. Wu, Y.; Xu, Z.; Liu, W.; Zhao, T.; Zhang, X.; Jiang, H.; Yu, C.; Zhou, L.; Zhou, X. Chemical compositions of precipitation at three non-urban sites of Hebei Province, North China: Influence of terrestrial sources on ionic composition. *Atmos. Res.* **2016**, *181*, 115–123. [CrossRef]
100. Balasubramanian, R.; Victor, T.; Chun, N. Chemical and Statistical Analysis of Precipitation in Singapore. *Water Air Soil Pollut.* **2001**, *130*, 451–456. [CrossRef]
101. Seinfeld, J. *Atmospheric Chemistry and Physics of Air Pollution*, 1st ed.; Wiley-Interscience: Cambridge, UK, 1986; Available online: https://pubs.acs.org/doi/pdf/10.1021/es00151a602 (accessed on 11 July 2022).